Joyashree Das, Rup Narayan Ray / International Journal of Engineering Research and Applications (IJERA) ISSN: 2248-9622 www.ijera.com
Vol. 2, Issue 5, September- October 2012, pp.1248-1257

Comparison of 2D and 3D Modeling of Hysteresis Motor with HTS Element in the Rotor

Joyashree Das (Research Scholar), Rup Narayan Ray (Associate Professor)
Deptt. of Electrical Engg., National Institute of Technology Agartala, Agartala-799055, INDIA.

Abstract

This paper presents 2D and 3D modeling of hysteresis motor using high temperature superconducting element Yttrium Barium Copper Oxide (YBCO) in the rotor. These hysteresis motors aim to improve the performance in comparison with that of conventional hysteresis motors. Various performance parameters of high temperature superconducting hysteresis motor are computed from the proposed 2D and 3D modeling. The hysteresis loop thus obtained is used to find torque and ac losses for variable applied current. The measured parameters are compared with the experimental data and both are found to be in good agreement. All the simulations are performed using MATLAB 7.5 and FEM based COMSOL Multiphysics software.

Keywords: High Temperature Superconducting (HTS) Hysteresis Motors, Yttrium Barium Copper Oxide (YBCO), Finite Element Method, COMSOL Multiphysics.

1. Introduction

Now-a-days, high temperature superconducting (HTS) hysteresis synchronous motors have received attention because of their economical advantage as well as noiseless operation, small size, self-starting torque and lightweight compared to the conventional motors [1]. The possibility of incorporating HTS into power applications such as electrical motors, generators, bearings and fault current limiters have attracted much attention. Hysteresis superconducting motors offer the simplest construction. Due to global interest along with industrial applications, the optimal performance study of the motor is most important. There are various techniques available to improve performance of the machine. The literature study regarding the performance improvement of the machine is presented in this section. The mathematical technique with type-II superconducting material in the rotor is developed based on the critical state model for obtaining the current and field distributions within the superconducting pieces using the finite element method [2]. The finite element analysis of hysteresis motor using magnetization-dependent model is employed as a hysteresis model. To find the efficient analysis method, various formulations are compared for hysteresis region and it is proved that pseudo-permeability method is most effective [3]. D. Inacio et al., investigated the numerical and experimental techniques for the comparison of both conventional and high temperature superconducting hysteresis motor. High temperature superconducting element (YBCO) is used as a rotor of HTS hysteresis motor and simulations are performed in finite elements software FLUX2D [4]. The drum and disc type hysteresis machine with superconducting rotors is proposed to obtain the optimal solution of the machine. For this analysis, finite element modeling software Flux2D was used [5]. The optimization technique of a coreless dual discs hysteresis motor (CDDHM) is developed using genetic algorithm [6]. A high efficiency operation scheme of a hysteresis motor is implemented which is driven by pulse width modulator (PWM) for a short duration over-excitation [7-9]. Changing magnetic property of the rotor using different types of rotor materials is one of the techniques to improve performance of the machine. Some of the examples are explained in this section using different materials.

In 1994, a new class of electromechanical converters type hysteresis machines is designed with solid high temperature superconducting material in the rotors. The comparative analysis of both the traditional and superconducting motor performance has been successfully carried out [10]. A cylindrical melt-textured YBCO blocks is used in the rotor of hysteresis motor. This motor presents the detailed investigation on magnetic processes in these rotors. It is also found that the construction of electro motors with increased power density is possible if HTS materials are used [11]. HTS electrical machines (hysteresis and reluctance machines) with YBCO materials in the rotor are developed and it is found that the specific output power of liquid nitrogen cooled HTS motors with bulk YBCO elements can be higher than the conventional motors [12]. Based on high temperature superconductors such as YBCO and Ag-BSCCO elements in the rotor of various shape, a new type of electrical motors is implemented. It is observed that the torque is linearly proportional to total hysteresis losses in the HTS rotor and independent on the rotor angular velocity [13-14]. An axial type HTS hysteresis motor is designed. In this HTS hysteresis motor, the rotor consists of BSCCO element with the objective

of increasing power densities and reducing losses. The experimental results are also presented for HTS hysteresis motor [1]. A HTS 150 kW reluctance motor is constructed with YBCO material that discussed the demands on YBCO bulk material in superconducting motor for high performance and also presents the conceptual design of a superconducting linear motor and future applications for superconducting motors of medium power range [15]. The performance of an axial type motor with a Bi-2223 HTS bulk rotor is fabricated and tested. It shows both the characteristics of conventional induction and hysteresis motor [16]. Radial flux type of hysteresis motor is also developed. In this motor, the rotor is made up of Fe-Cr-Co magnet steel [17]. The operation principle and theoretical aspects of both the conventional and HTS hysteresis motors are discussed. In this type of HTS hysteresis motor, YBCO element is used in the rotor. The characteristics of both motors are implemented and compared. It shows that the torque and power ranges of HTS hysteresis motor are usually higher than the conventional hysteresis motor [4]. Due to the simple construction of HTS hysteresis machines, superconducting (YBCO) rotor is used in drum and disc type of hysteresis machines. The torque of HTS hysteresis motor produces from the repulsion of the magnetic poles induced into the HTS rotor by the rotating field of the stator winding [5].

Several international research groups have explored the use of HTS materials in the construction of rotor of hysteresis motors [5], as superconducting materials has the ability to trap the higher magnetic field, higher flux density and carries greater current density at higher magnetic field, high magnetic permeability, high saturation magnetization consequently the developed power also gets increased. Some exclusive superiority of superconducting synchronous machines over its conventional machines have better torque to volume ratio [4-5], compact size, light weight and reduced losses for the same power [4],[18]. During last two decades, different types of hysteresis machines have been constructed successfully [19-22].

There are several simulation tools available to model the HTS hysteresis motor using finite element method (FEM) [5]. For the purpose of analysis, 2D modeling of the machine is generally adopted. However, 2D modeling of HTS hysteresis motor has the limitation to analyze performance of the machine. Due to the rotation of the magnetic domains, magnetic material shows 3D magnetic property even under 2D rotating magnetic excitation. The modeling and analysis of magnetization process of the motor can be completed if 3D properties are properly considered. It calculates the magnetic fields around and inside the motor. A better precision may be obtained if 3D modeling is incorporated for the purpose of performance analysis, which is not reported until now. Hence, 3D modeling of HTS hysteresis motor is proposed which is more precise and realistic and very useful in simulations. This paper is organized as follows: Section 2 describes about the modeling of hysteresis motor. In Section 3, simulation and experimental results are shown, and finally, conclusions are drawn in Section 4.

2. Modeling of Hysteresis Motor

2.1. Conventional hysteresis motor

The topology of hysteresis motor is shown in Fig. 1. The main parts of hysteresis motor are stator and rotor. In this motor, the armature winding is built in the stator slots and it consists of conventional copper conductors to create the magnetic rotating field and the stator core is made of iron. The rotor of this type motor consists of hard iron ring with a high degree of magnetic hysteresis. Due to the use of magnetic materials in the rotor, there is no dc excitation in the rotor. The shaft is made up of paramagnetic material [4].

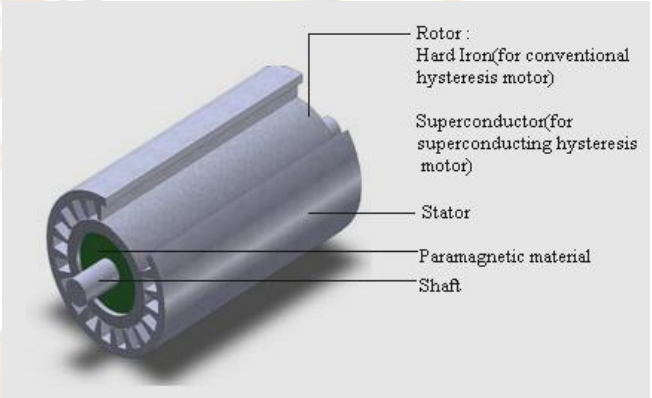

Fig. 1. Hysteresis motor layout [4].

2.2. 2D modeling of HTS hysteresis motor

The schematic diagram of HTS hysteresis motor is shown in Fig. 2. Superconducting hysteresis motor is almost identical with conventional hysteresis motor but its rotor is made up of HTS materials (YBCO). The rotor core is constructed with paramagnetic materials. In this HTS hysteresis motor aluminum is used as a paramagnetic material only for mechanical support of the HTS elements [5]. In this case the shaft also consists of paramagnetic material and steel is used as a paramagnetic material. A single superconducting cylinder cannot be constructed due to the brittle nature of YBCO materials. So the segments are assembled with epoxy resin [4], [5]. Huge numbers of segments are advantageous for large shielding [2]. If the numbers of the circular sectors are increased, the flux distribution inside the HTS rotor is also increased because of the presence of paramagnetic materials between them. But the

numbers of circular sectors are limited, otherwise flux leakage increases with increase of the number of sectors and thus the developed torque of the hysteresis motor will decrease [5].

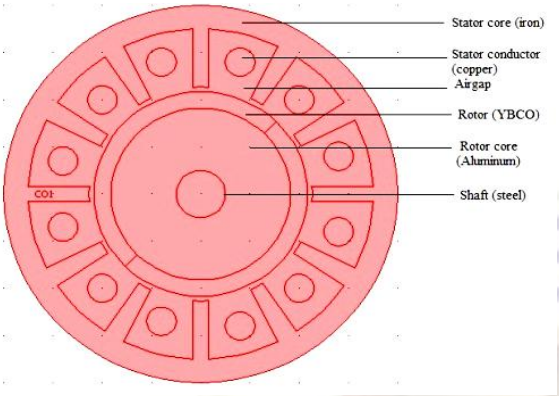

Fig. 2. Schematic diagram of HTS hysteresis motor in COMSOL MULTIPHYSICS.

2.3. Proposed 3D modeling of HTS hysteresis motor

3D HTS hysteresis motor has the same materials and specifications as 2D HTS hysteresis motor except the motor is replaced by the 3-dimentional model. The 3D view of HTS hysteresis motor is shown in Fig. 3.

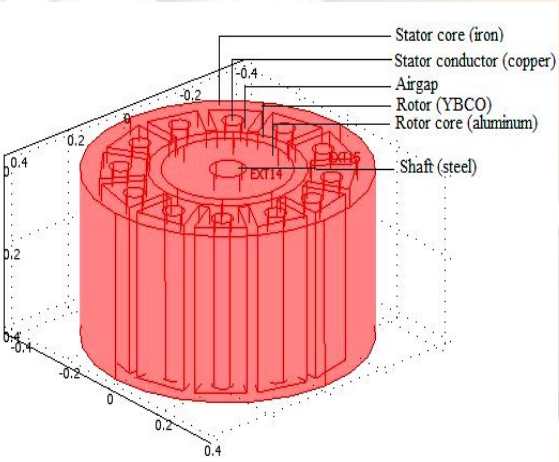

Fig. 3. 3-dimentional view of HTS hysteresis motor in COMSOL MULTIPHYSICS.

The hysteresis loop is the most important phenomenon in any hysteresis motor and *E-H* formulation is the most useful expression of an electromagnetic field [23]. Therefore, the basic electromagnetic equation for the HTS hysteresis motor is

$$\nabla \times E = -\partial \vec{B}/\partial t \qquad (1)$$

Where, E is electric field (V/m) and B is magnetic flux density (T).

Therefore, $\nabla^2 \vec{H} - \mu\sigma\left(\partial \vec{H}/\partial t\right) = 0$ (2)

Here, H is magnetic field (A/m), $H = \begin{bmatrix} Hx \\ Hy \end{bmatrix}_{2D}$ and

$\begin{bmatrix} Hx \\ Hy \\ Hz \end{bmatrix}_{3D}$

Where, μ is permeability (H/m), σ is conductivity (S/m) and B_r is residual flux density (T) respectively.

After determine the value of H, the value of current density (J) is obtained using the following equation

$$\vec{J} = \nabla \times \vec{H} \qquad (3)$$

Then the electric field E is calculated using the *E-j* power law

$$E = Ec\left(\vec{J}/J_c\right)^n \qquad (4)$$

Where, E_c is critical electric field (V/m), J_c is critical current density (A/m^2) and n is power index respectively.

After determining E and J, total ac loss Q is obtained by

$$Q = 1/T \int_0^T \int_s (J \cdot E) ds dt \qquad (5)$$

Where, T is time period.

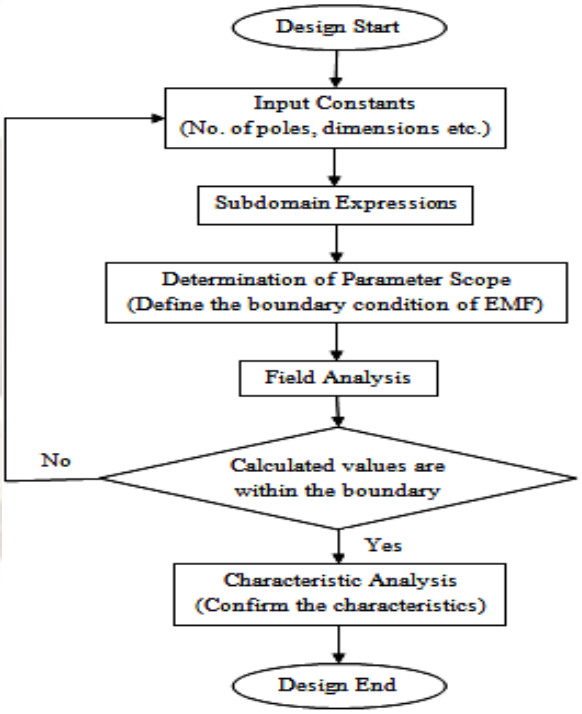

Fig. 4. Flow chart

3. Simulation and Experimental Results

Both 2D and 3D high temperature superconducting hysteresis motors are numerically simulated using the software COMSOL Multiphysics and based on finite element method.

The *E-j* power law derived in Eq. (4) and it is used to calculate the ac losses of HTS hysteresis motor. The specifications of the high temperature superconducting material used in the rotor of the HTS hysteresis motor is shown in Table 1 and also the dimensions of the conventional and HTS hysteresis motor is shown in Table 2.

Table 1. Specifications of the HTS material used in the rotor.

Name of the sample	YBCO
Outer radius(*cm*)	2.17
Inner radius(*cm*)	1.82
Thickness(*cm*)	0.35
Critical electric field(*V/m*)	10^{-4}
Initial Conductivity (*S/m*)	10^{16}
Critical current density(A/m^2)	4×10^{7}

Table 2. Dimensions of HTS and conventional hysteresis motor.

Dimensions	HTS hysteresis motor (*cm*)	Conventional hysteresis motor (*cm*)
Stator Outer Radius	4	6
Rotor Outer Radius	2.17	2.8
Rotor Inner Radius	1.82	2.625
Air-gap	0.1	0.1

The mesh statistics are applied to discretized the HTS hysteresis motor into finite elements. In order to have high level of accuracy the automatic mesh diagram is not used and a mesh diagram is designed manually. In this simulation, the numbers of nodes are higher around the air gap and hysteresis rotor. From this mesh statistics, various parameters are known, shown in Table 3.

Table 3. Mesh statistics of HTS hysteresis motor

Mesh statistics	2D	3D
Mesh	Triangular	Tetrahedral
Number of elements	17432	23564
Number of degrees of freedom	34754	100531
Number of boundary elements	1234	5012
Solution time (*s*)	26.219	94.9282

The solution time is changed due to change in the values of various parameters but the number of elements and number of degrees of freedom will remain same unless the geometry is changed. Fig. 5 shows the mesh of a 2D and 3D HTS hysteresis motor.

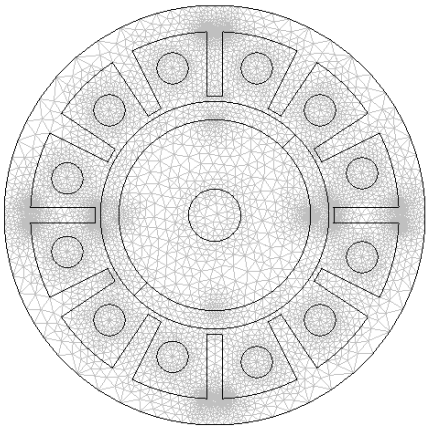

2D

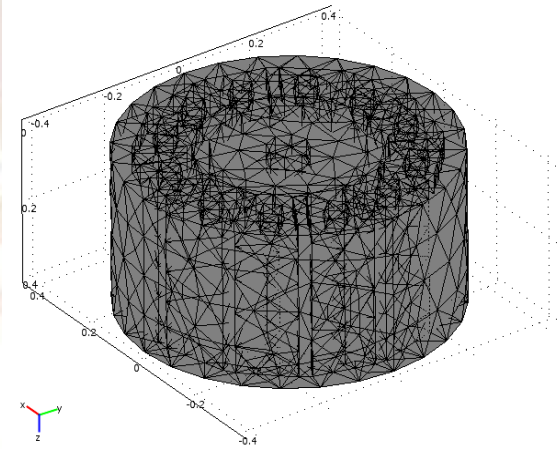

3D

Fig. 5. Mesh of 2D and 3D HTS hysteresis motor.

3.1. Magnetic flux distribution in HTS hysteresis motor

Fig. 6 shows the streamline plot of magnetic flux density in a 2D and 3D HTS hysteresis motor. It is observed that two poles have been created in both 2D and 3D HTS hysteresis motor and also three-dimensional model calculates magnetic fields around and inside the hysteresis motor. The transport current of non-HTS stator produces rotating field in the air gap between the stator and the rotor of the motor, which in turn induces currents in the superconductor and thus the HTS rotor is magnetized. Because of the high current leading ability of the HTS material, most of the fluxes are trapped in the HTS hysteresis rotor. This phenomenon is shown in the plots of flux density (*B*) and magnetic field (*H*) in 2D and 3D HTS hysteresis motor in Fig. 7 and Fig. 8. From Fig. 7 and Fig. 8, it is observed that compared to the other region the magnetic flux concentration is more inside the HTS rotor and the flux density and magnetic field in 3D HTS hysteresis motor is higher

than 2D HTS hysteresis motor for the same condition.

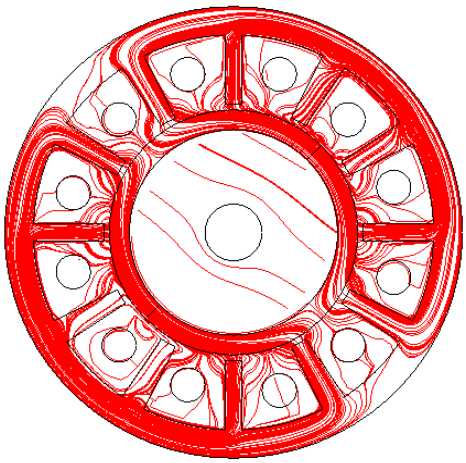

2D

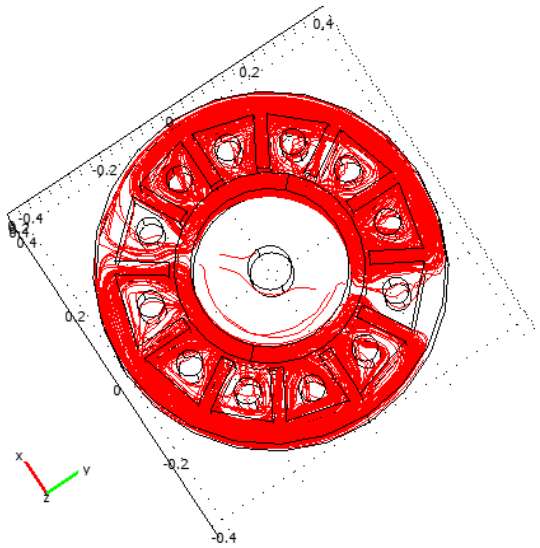

3D

Fig. 6. Streamline plot of magnetic flux density of a 2D and 3D HTS hysteresis motor.

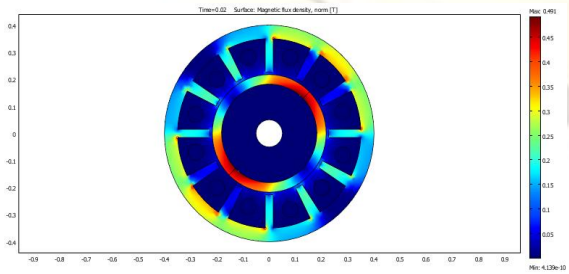

a

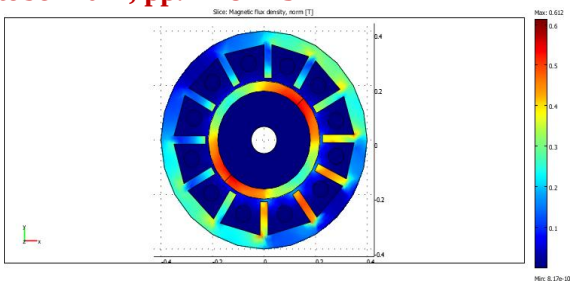

b

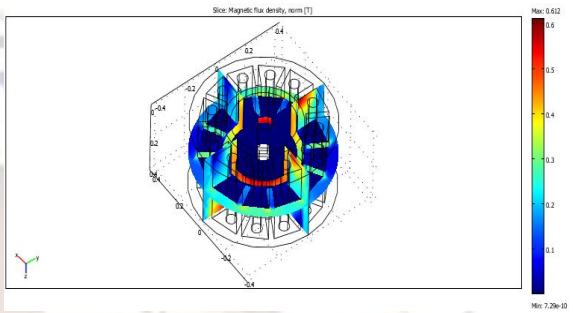

c

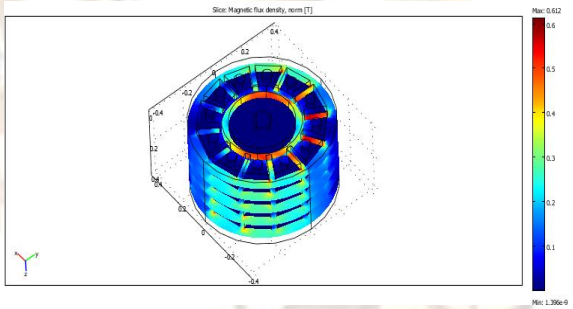

d

Fig.7. a. Magnetic flux density (*B*) plot of a 2D HTS hysteresis motor, **b.** Magnetic flux density (*B*) (Top view) plot of a 3D HTS hysteresis motor, **c.** Magnetic flux density (*B*) [at (1,1,1)] plot of a 3D HTS hysteresis motor, **d.** Magnetic flux density (*B*) plot of a 3D HTS hysteresis motor (at level 5).

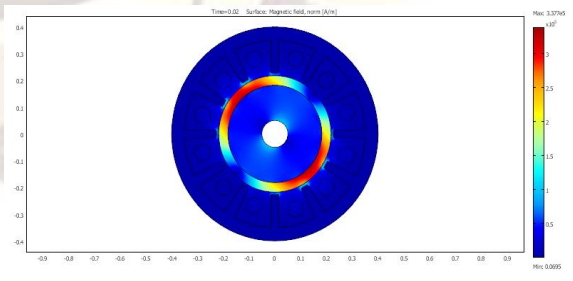

a

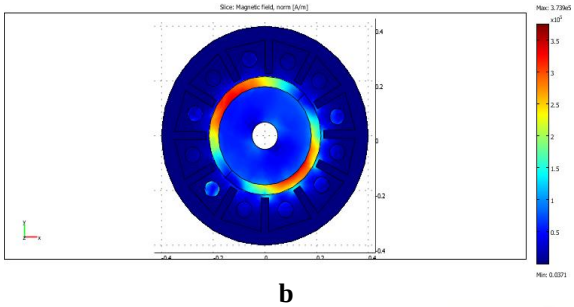

b

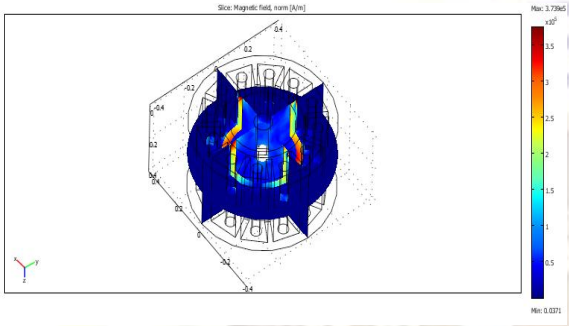

c

Fig. 8. a. Magnetic field (*H*) plot of a 2D HTS hysteresis motor, **b.** Magnetic field (*H*) [at (1,1,0)] plot of a 3D HTS hysteresis motor, **c.** Magnetic field (*H*) at (1,1,1) plot of a 3D HTS hysteresis motor.

3.2. Hysteresis loop of HTS hysteresis motor

Due to the application of variable transport currents of different magnitudes in the non-HTS stator conductors, different flux plots are obtained. The values of magnetic fields (*H*) and the flux densities (*B*) at different positions on the HTS rotor have been taken and then the hysteresis loops are plotted. The areas of the hysteresis loops Fig. 9 are changed at different stator current. Due to the higher value of magnetic field and flux density in 3D HTS hysteresis motor than 2D HTS hysteresis motor, the area of the 3D hysteresis loops are larger than the 2D hysteresis loops shown in Fig. 9. When the applied current in the stator is increased resulting the increase of field strength of rotating magnetic field in the air gap, more fluxes are trapped into the HTS material. The area of the hysteresis loop is also increased and thus the power density of the hysteresis motor is increased.

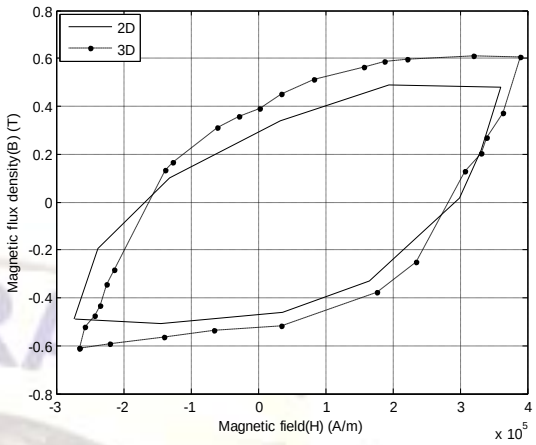

Fig. 9. B-H loop of a 2D and 3D HTS hysteresis motor.

3.3. Effects of applied current on torque of a HTS hysteresis motor

The area of hysteresis loop is approximately proportional to the applied current that is calculated in the last section. It is also known that the torque is directly proportional to the area of the hysteresis loop. Therefore, the torque is directly proportional to the current. The torque in hysteresis motor is calculated using the relation, $T = \left(\frac{1}{2\Pi}\right) P V_r A_h$, [3] where, P is number of pole pairs, V_r is volume of the HTS rotor and A_h is area of the hysteresis loop in the HTS rotor. MATLAB program has been developed to draw the hysteresis curves and the corresponding torque developed in the motor. As shown in Fig. 10, the torque changes almost linearly with the applied current and that is the common feature of any hysteresis motor [3], because of the area of the hysteresis loop is approximately proportional to the applied current. It is also observed that the value of torque in 3D HTS hysteresis motor is higher than 2D HTS hysteresis motor as well as conventional hysteresis motor. The simulation result shows a good agreement with the experimental results of a conventional hysteresis motor [3], [24-25] as shown in Table 4.

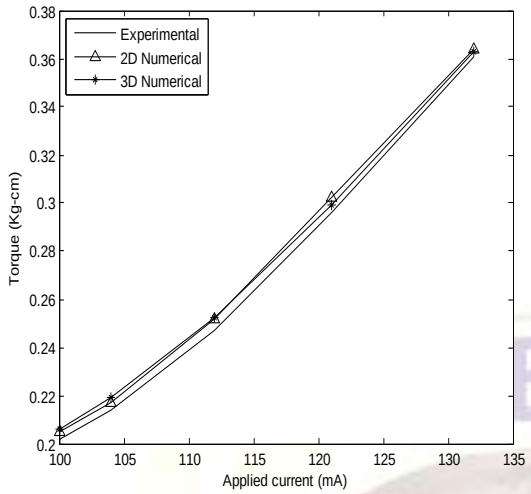

Fig. 10. Torque vs. current of 2D and 3D HTS hysteresis motor.

Table 4. Comparison between 2D, 3D HTS and conventional hysteresis motor.

Parameter	2D (HTS)	3D (HTS)	Experimental (Conventional)
Torque (*Kg-cm*)	0.2664	0.2679	0.2647

3.4. Current density plot in a HTS hysteresis motor

The Fig. 11 shows the current density plot of a 2D and 3D HTS hysteresis rotor. Due to the trapped field effect in the HTS hysteresis rotor, the current density also more in that region but it is not uniform due to the anisotropic conductivity of the superconducting material. When the trapped fields are gradually decreased in the inner part of the HTS rotor, the current density also gradually decreases and becomes minimum in the inner part of the rotor. In both of the HTS hysteresis motors, the value of power index (*n*) is 15 and the value of integral of current density in the 2D HTS rotor is $3.076916\times10^{6}\,A/m^{2}$ and 3D HTS rotor is $8.34053\times10^{6}\,A/m^{2}$. It is observed that the value of integral of current density is less compared to the critical current density ($4\times10^{7}\,A/m^{2}$) and it is also observed that the current density in 3D HTS hysteresis motor is higher than 2D HTS hysteresis motor.

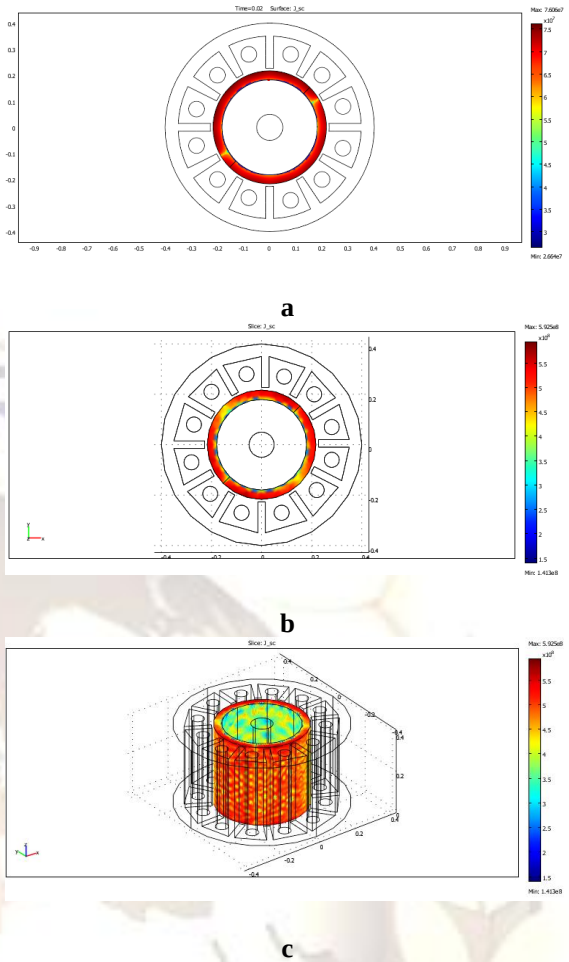

a

b

c

Fig. 11. a. Current density plot of a 2D, **b.** current density (top view), **c.** current density plot 3D HTS hysteresis rotor.

3.5. Losses in a HTS hysteresis motor

It is known that the torque is directly proportional to the hysteresis loss in the superconducting element [4]. Thus, the loss can also be calculated from the torque and it is independent of the field rotational frequency [1]. This torque is already calculated in last section. When the applied current is increased, the HTS have the trend to either have a larger amount of current or greater volume of current. When the HTS is in maximum current carrying condition, there is no additional volume for the new current to flow, thus the magnitude of current will increase. According to *E-j* power law, when applied current increases, the current density and electric field is also increased as a result of this the value of AC loss (*Q*) is also increased following eq. (5), which is proportional to the product of *E* and *J*. The AC losses have been calculated with different peak values of applied current, shown in Fig. 12. This is because the *E-j* power law is used with the power index *n*=15. From this plot, it is observed that the AC loss increases with the increase of applied current.

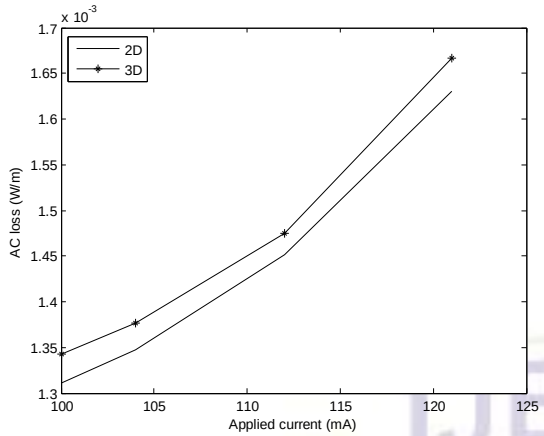

Fig. 12. AC loss vs. applied current of 2D and 3D HTS hysteresis motor.

Table 5. Comparison between 2D and 3D HTS hysteresis motor.

Parameters	2D	3D
AC loss(*W/m*)	1.4348e-3	1.4753e-3
Current density (A/mm^2)	3.076916	8.340531

4. Conclusion

In this work, modeling of 2D and 3D hysteresis motors using HTS material are presented and the computed parameters are compared with the experimental ones. All the simulated results show a good matching with the experimental results and it also shows that the bulk HTS material can trap higher value of magnetic field compared to ferro-magnetic material. The three dimensional model calculates magnetic fields around and inside the motor and gives better results of motor performance. It has been observed that the developed torque increases almost linearly with the increase of the applied current. Three dimensional modeling of HTS hysteresis motor is proposed which is more precise and realistic and very useful in simulations. The proposed 3D modeling of HTS hysteresis motor gives superior results compared to 2D modeling as far as the experimental results are concerned.

References

[1] Muta, I., Jung, H. J., Hirata, T., Nakamura, T., Hoshino, T., & Konishi, T. (2001). Fundamental experiments of axial-type BSCCO-bulk superconducting motor model. *IEEE Transactions On Applied Superconductivity, II (I),* 1964-1967.

[2] Barnes, G. J., McCulloch, M. D., & Dew-Hughes, D. (2000). Torque from hysteresis machines with type-II superconducting segmented rotors. *Physica C: Superconductivity, 331(2),* 133-140.

[3] Hong-Kyu, Kim, Sun-Ki, Hong, & Hyun-Kyo, J. (2000). Analysis of hysteresis motor using finite element method and magnetization-dependent model. *IEEE Transactions On Magnetics, 36(4),* 685-688.

[4] Inacio, D., Inacio S., Pina, J., Goncalves, A., Ventim, Neves, M., & Rodrigues, Leao, A. (2007). Numerical and experimental comparison of electromechanical properties and efficiency of HTS and ferromagnetic hysteresis motors. *8th European Conference On Applied Superconductivity (EUCAS 2007),* 1-7.

[5] Rodrigues, Leao, A. (2009). Drum and disc type hysteresis machines with superconducting rotors. *IEEE,* 55-59.

[6] Sadeghi, H., M., & Darabi, A. (2010). Optimization of a new type of hysteresis motor using genetic algorithm. *EEEIC,* 479-482.

[7] Kubota, T., Tamura, T., & Kurihara, K. (2009). High-efficiency operation of PWM inverter-driven hysteresis motor with short-duration overexcitation. *Proc. Int. Conf. Elect. Mach. And Systems,* 1-4.

[8] Kubota, T., Tamura, T., & Kurihara, K. (2010). New scheme for high-efficiency operation of PWM inverter-driven hysteresis motor with short-duration overexcitation. *International Conference on Electrical Machines,* 1-6.

[9] Kubota, T., Tamura, T., & Kurihara, K. (2010). Characteristics of PWM inverter-driven hysteresis motor with short-duration overexcitation. *ICEMS,* 1429-1433.

[10] Kovalev, L., K., Ilyushin, K., V., Penkin, V., T., & Kovalev, K., L. (1994). Hysteresis machines with high temperature superconducting rotors. *Elsevier Science,* 145-170.

[11] Habisreuther, T., Strasser, T., Gawalek, W., Goorner,t P., Ilushin, K., V., & Kovalev, L., K. (1997). Magnetic processes in hysteresis motors equipped with melt-textured YBCO. *IEEE Transactions On Applied Superconductivity, 7(2),* 900-903.

[12] Kovalev, L., K., Ilushin, K., V., Koneev, S., M., A., Kovalev, K., L., Penkin, V., T., Poltavets, V., N., Gawalek, W., Habisreuther, T., Oswald, B., & Best, K., J. (1999). Hysteresis and reluctance electric machines with bulk HTS rotor elements. *IEEE Transactions On Applied Superconductivity, 9(2),* 1261-1264.

[13] Kovalev, L., K., Ilushin, K., V., Kovalev, K., L., Penkin, V., T., Poltavets, V., N.,

Gawalek, W., & Habisreuther, T. et al. (1998). Hysteresis electrical motors with bulk melt texture YBCO. *Material Science and Engineering*, 216-219.

[14] Kovalev, L., K., Ilushin, K., V., Koneev, S., M., A., Kovalev, K., L., Penkin, V., T., Modestov, A., K., Larionoff, A., S., Gawalek, W., & Oswald, B. (2001). HTS electrical machines with YBCO bulk and Ag-BSCCO plate-shape HTS elements: recent results and future development. *Physica C: Superconductivity, 354(1-4)*, 34-39.

[15] Oswald, B., Krone, M., Strasser, T., Best, K., J., & Soil, M. et al. (2002). Design of HTS reluctance motors up to several hundred kW. *Physica C: Superconductivity, 372-376 (2)*, 1513-1516.

[16] Muta, I., Jung, H., Nakamura, T., & Hoshino, T. (2002). Performance of axial-type motor with Bi-2223 HTS bulk rotor. *Physica C: Superconductivity, 372-376(3)*, 1531-1534.

[17] Wakui, G., Kurihara, K., & Kubota, T. (2007). Radial flux type hysteresis motor with rotor ring of sprayed surface layer. *Electrical Engineering in Japan, 112(4)*, 132-143.

[18] Match, L., & Morgan, J. (1986). *Electromagnetic and Electromechanical Machines.* Wiley & Sons.

[19] McCulloch, M., & Dew-Hughes, D. (1998). Brushless ac machines with high temperature superconducting rotors. *Material Science and Engineering B53*, 211-215.

[20] Chun, Y. D., Kim, Y. H., Lee, J., Hong, J. P., & Lee, J. W. (2001). Finite element analysis of magnetic field in high temperature bulk superconductor. *IEEE Trans. On Applied Superconductivity 11(1), 11(2)*, 2000-2003.

[21] Suguira, T., Shashizume, H., and Mika, K. (1991). Numerical electromagnetic field analysis of type II superconductors. *Int J. of Applied Electromagnetics in Materials 2*, 183.

[22] Nakamura, T. et al. (2004). Synchronization of an axial type Bi2223 bulk motor operated in liquid nitrogen. *Superconductor Science and Technology 17*, 1319-1323.

[23] Chari, M. V. K., and Silvester, P. P. (1980). *Finite Elements in Electrical and Magnetic Field Problems.* New York: John Willy and Sons, 31-36.

[24] Sun-Ki, Hong, Hong-Kyu, Kim, Hyeong-Seok, Kim, & Hyun-Kyo, J. (2000). Torque calculation of hysteresis motor using vector hysteresis model. *IEEE Transactions On Magnetics, 36(4)*, 1932-1935.

[25] Lee, Hak-Yong, Hahn, Song-yop, Park, Gwan-Soo, & Lee, Ki-Sik (1998). Torque computation of hysteresis motor using finite element analysis with asymmetric two dimensional magnetic permeability tensor. *IEEE Transactions On Magnetics, 34(5)*, 3032-3035.